Functional Connectivity Abnormalities of the Subgenual Anterior Cingulate Cortex: Implications for Transcranial Magnetic Stimulation in Depression

Xiao Chen[1,2,3,4,5]#, Bin Lu[1,3,4,5]#, Yu-Wei Wang[1,3,4,5], Xue-Ying Li[1,3,4,5], Zi-Han Wang[1,3,4,5], Hui-Xian Li[6], Yi-Fan Liao[1,3,4,5], Daniel M. Blumberger[2,7], Francisco Xavier Castellanos[8,9], Li-Ping Cao[10], Guan-Mao Chen[11], Jian-Shan Chen[10], Tao Chen[12], Tao-Lin Chen[13,14] , Yan-Rong Chen[1,3,4,5], Yu-Qi Cheng[15], Zhao-Song Chu[15], Shi-Xian Cui[1,16,17], Xi-Long Cui[18], Zhao-Yu Deng[1,3,4,5], Qing-Lin Gao[1,3,4,5], Qi-Yong Gong[13,14], Wen-Bin Guo[18], Can-Can He[19], Zheng-Jia-Yi Hu[1,16,17], Qian Huang[20], Xin-Lei Ji[18], Feng-Nan Jia[21], Li Kuang[20], Bao-Juan Li[22], Feng Li[23], Tao Li[24,25] , Xue Li[1,3,4,5], Tao Lian[1,3,4,5], Xiao-Yun Liu[26], Yan-Song Liu[21], Zhe-Ning Liu[18], Yi-Cheng Long[18], Jian-Ping Lu[27], Jiang Qiu[28], Xiao-Xiao Shan[18], Tian-Mei Si[29], Peng-Feng Sun[30], Chuan-Yue Wang[23], Han-Lin Wang[1,3,4,5], Hua-Ning Wang[22], Xiang Wang[18], Ying Wang[11], Chen-Nan Wu[1,3,4,5], Xiao-Ping Wu[30], Xin-Ran Wu[28], Yan-Kun Wu[29], Chun-Ming Xie[19], Guang-Rong Xie[18], Peng Xie[31,32,33] , Xiu-Feng Xu[15], Zhen-Peng Xue[27], Hong Yang[12], Jian Yang[32], Hua Yu[24,25], Yong-Qiang Yu[34,35,36], Min-Lan Yuan[37], Yong-Gui Yuan[26], Yu-Feng Zang[38,39] , Ai-Xia Zhang[40], Ke-Rang Zhang[40], Wei Zhang[37], Zi-Jing Zhang[1,3,4,5], Jing-Ping Zhao[18], Jia-Jia Zhu[34,35,36], Xi-Nian Zuo[41,42], the DIRECT Consortium, Chao-Gan Yan[1,3,4,5,16,17]*

[1]CAS Key Laboratory of Behavioral Science, Institute of Psychology, Beijing 100101, China

[2]Temerty Centre for Therapeutic Brain Intervention, Campbell Family Research Institute, Centre for Addiction and Mental Health, Toronto, Ontario M6J1H4, Canada

[3]Magnetic Resonance Imaging Research Center, Institute of Psychology, Chinese Academy of Sciences, Beijing 100101, China

[4]Department of Psychology, University of Chinese Academy of Sciences, Beijing 100049, China

[5]International Big-Data Center for Depression Research, Chinese Academy of Sciences, Beijing 100101, China

[6]The Third Affiliated Hospital of Zhengzhou University, Zhengzhou, Henan 450052, China

[7]Department of Psychiatry, Temerty Faculty of Medicine, University of Toronto, Toronto, Ontario M5S1A1, Canada

[8]Department of Child and Adolescent Psychiatry, NYU Grossman School of Medicine, New York, NY

29 10016, USA

30 [9]Nathan Kline Institute for Psychiatric Research, Orangeburg, NY 10962, USA

31 [10]Affiliated Brain Hospital of Guangzhou Medical University, Guangzhou, Guangdong 510370, China

32 [11]The First Affiliated Hospital of Jinan University, Guangzhou, Guangdong 250024, China

33 [12]Department of Radiology, The First Affiliated Hospital, College of Medicine, Zhejiang University,

34 Hangzhou, Zhejiang 310058, China

35 [13]Huaxi MR Research Center (HMRRC), Department of Radiology, West China Hospital of Sichuan

36 University, Chengdu, Sichuan 610044, China

37 [14]Research Unit of Psychoradiology, Chinese Academy of Medical Sciences, Chengdu, Sichuan 610052,

38 China

39 [15]Department of Psychiatry, First Affiliated Hospital of Kunming Medical University, Kunming, Yunnan

40 650032, China

41 [16]Sino-Danish College, University of Chinese Academy of Sciences, Beijing 101408, China

42 [17]Sino-Danish Center for Education and Research, Graduate University of Chinese Academy of Sciences,

43 Beijing 101408, China

44 [18]Department of Psychiatry, and National Clinical Research Center for Mental Disorders, The Second

45 Xiangya Hospital of Central South University, Changsha, Hunan 410011, China

46 [19]Department of Neurology, Affiliated ZhongDa Hospital of Southeast University, Nanjing, Jiangsu

47 210009, China

48 [20]Department of Psychiatry, The First Affiliated Hospital of Chongqing Medical University, Chongqing

49 400042, China

50 [21]Department of Clinical Psychology, Suzhou Psychiatric Hospital, The Affiliated Guangji Hospital of

51 Soochow University, Suzhou, Jiangsu 215003, China

52 [22]Xijing Hospital of Air Force Military Medical University, Xi'an, Shaanxi 710032, China

53 [23]Beijing Anding Hospital, Capital Medical University, Beijing 100120, China

54 [24]Affiliated Mental Health Center & Hangzhou Seventh People's Hospital, Zhejiang University School of

55 Medicine, Hangzhou, Zhejiang 310063, China

56 [25]Mental Health Center and Psychiatric Laboratory, West China Hospital of Sichuan University,

57 Chengdu, Sichuan 610044, China

58 [26]Department of Psychosomatics and Psychiatry, Zhongda Hospital, School of Medicine, Southeast
59 University, Nanjing, Jiangsu 210009, China
60 [27]Shenzhen Kangning Hospital, Shenzhen, Guangzhou 518020, China
61 [28]Faculty of Psychology, Southwest University, Chongqing 400715, China
62 [29]National Clinical Research Center for Mental Disorders (Peking University Sixth Hospital) & Key
63 Laboratory of Mental Health, Ministry of Health (Peking University), Beijing 100191, China
64 [30]Xi'an Central Hospital, Xi'an, Shaanxi 710004, China
65 [31]Institute of Neuroscience, Chongqing Medical University, Chongqing 400016, China
66 [32]Chongqing Key Laboratory of Neurobiology, Chongqing 400000, China
67 [33]Department of Neurology, The First Affiliated Hospital of Chongqing Medical University, Chongqing
68 400042, China
69 [34]Department of Radiology, The First Affiliated Hospital of Anhui Medical University, Hefei, Anhui
70 230022, China
71 [35]Research Center of Clinical Medical Imaging, Hefei, Anhui 230032, China
72 [36]Anhui Provincial Institute of Translational Medicine, Hefei, Anhui 230032, China
73 [37]West China Hospital of Sichuan University, Chengdu, Sichuan 610044, China
74 [38]Center for Cognition and Brain Disorders, The Affiliated Hospital of Hangzhou Normal University,
75 Hangzhou, Zhejiang 310018, China
76 [39]Zhejiang Key Laboratory for Research in Assessment of Cognitive Impairments, Hangzhou, Zhejiang
77 310000, China
78 [40]First Hospital of Shanxi Medical University, Taiyuan, Shanxi 030001, China
79 [41]Developmental Population Neuroscience Research Center, IDG/McGovern Institute for Brain
80 Research, Beijing Normal University, Beijing 100091, China
81 [42]National Basic Science Data Center, Beijing 100038, China
82 [43]Department of Psychiatry, Sir Run Run Shaw Hospital, Zhejiang University School of Medicine,
83 Hangzhou, Zhejiang 310020, China
84 [44]Shanghai Mental Health Center, Shanghai Jiao Tong University School of Medicine, Shanghai 200030,
85 China
86 [45]Department of Diagnostics, Affiliated Hospital, Hangzhou Normal University Medical School,

Hangzhou, Zhejiang 311121, China

[46]Department of Psychiatry, First Affiliated Hospital, China Medical University, Shenyang, Liaoning 110122, China

[47]Early Intervention Unit, Department of Psychiatry, Affiliated Nanjing Brain Hospital, Nanjing Medical University, Nanjing, Jiangsu 210024, China

[48]Department of Neurology, The First Affiliated Hospital of Anhui Medical University, Hefei, Anhui 230022, China

[49]Department of Psychiatry, Shanghai Jiao Tong University School of Medicine, Shanghai 200025, China

*Corresponding author:

Chao-Gan Yan, Ph. D.

CAS Key Laboratory of Behavioral Science, Institute of Psychology, Beijing, China

16 Lincui Road, Chaoyang District, Beijing 100101, China

Tel: +86-10-64101582

E-mail: yancg@psych.ac.cn

#Xiao Chen and Bin Lu contributed equally to this work.

DIRECT consortium: Chao-Gan Yan, Ph.D.[1,3,4,5,16,17], Xiao Chen, Ph.D.[1,2,3,4,5], Li-Ping Cao, M.D.[10], Wei Chen, M.D.[43], Yu-Qi Cheng, M.D.[15], Yi-Ru Fang, M.D.[44], Qi-Yong Gong, M.D.[13,14], Wen-Bin Guo, M.D.[18], Li Kuang, M.D.[20], Bao-Juan Li, M.D.[22], Tao Li, M.D.[24,25], Yan-Song Liu, M.D.[21], Zhe-Ning Liu, M.D.[18], Jian-Ping Lu, M.D.[27], Qing-Hua Luo, M.D.[20], Hua-Qing Meng, M.D.[20], Dai-Hui Peng, M.D.[44], Jiang Qiu, Ph.D.[28], Yue-Di Shen, M.D.[45], Tian-Mei Si, M.D.[29], Yan-Qing Tang, M.D.[46], Chuan-Yue Wang, M.D.[23], Fei Wang, M.D.[46,47], Hua-Ning Wang, M.D.[22], Kai Wang, M.D.[48], Xiang Wang, M.D.[18], Ying Wang, M.D.[11], Xiao-Ping Wu, M.D.[30], Chun-Ming Xie, M.D.[19], Guang-Rong Xie, M.D.[18], Peng Xie, M.D.[31,32,33], Xiu-Feng Xu, M.D.[15], Hong Yang, M.D.[12], Jian Yang, M.D.[32], Shu-Qiao Yao, M.D.[18], Yong-Qiang Yu, M.D.[34,35,36], Yong-Gui Yuan, M.D.[26], Ke-Rang Zhang, M.D.[40], Wei Zhang, M.D.[37], Zhi-Jun Zhang, M.D.[19], Jun-Juan Zhu, M.D.[49], Xi-Nian Zuo, Ph.D.[41,42], Jing-Ping Zhao, M.D.[18], Yu-Feng Zang, M.D.[38,39]

Abstract

Background: The subgenual anterior cingulate cortex (sgACC) plays a central role in the pathophysiology of major depressive disorder (MDD), and its functional interactive profile with the left dorsal lateral prefrontal cortex (DLPFC) is associated with transcranial magnetic stimulation (TMS) treatment outcomes. Nevertheless, previous research on sgACC functional connectivity (FC) in MDD has yielded inconsistent results, partly due to small sample sizes and limited statistical power. Furthermore, calculating sgACC-FC to target TMS on an individual level is challenging because of the low signal-to-noise ratio and the poor replicability of individualized functional brain images.

Methods: Leveraging a large multi-site cross-sectional sample (1660 MDD patients vs. 1341 healthy controls) from Phase II of the Depression Imaging REsearch ConsorTium (DIRECT), we systematically delineated case-control difference maps of sgACC-FC. Then, in a sample of 25 individuals with treatment-resistant depression who had received repetitive TMS (rTMS) treatment, we examined the relationship between case-control differences in FCs between sgACC and their specific TMS targets and treatment outcomes. Next, we tested whether the position of the group mean FC-based target (previously determined in healthy participants) differed in MDD patients. Finally, we developed a dual regression (DR) based approach to integrate group-level statistical maps with individual-level spontaneous brain activity to evaluate individualized TMS target localization in MDD. We tested this approach in a sample of 16 individuals who had received rTMS.

Results: We found enhanced sgACC-DLPFC FC in MDD patients. The magnitude of case-control differences in FC between sgACC and TMS targets was related to clinical improvement. We found different peak sgACC anticorrelation locations in mean FC maps of MDD patients and HCs. More effective TMS targets were closer to individualized DR-based loci than to group-level targets.

Conclusion: In summary, we reliably delineated MDD-related abnormalities of sgACC-FC profiles in a large independently ascertained sample and demonstrated the potential impact of such case-control differences on FC-guided localization of TMS targets. The proposed

individualized approach for TMS targeting has the potential to improve TMS treatment outcome and warrants prospective clinical trials.

Keywords: major depressive disorder, transcranial magnetic stimulation, individualization, subgenual anterior cingulate cortex, functional connectivity, dual regression

149 **Introduction**

150 Major depressive disorder (MDD) is a common and debilitating psychiatric disorder projected
151 to be the most burdensome condition worldwide by 2030 [1]. Despite extensive research, the
152 pathophysiology of MDD remains elusive. Nevertheless, a key putative brain region appears
153 to be the subgenual anterior cingulate cortex (sgACC), which shows reproducible metabolic
154 hyperactivity [2], is targeted by effective deep brain stimulation [3,4], and has been implicated in
155 emotional responses, motivation, and rumination [5]. Accordingly, identifying an optimized
156 neuromodulation target in the left dorsal lateral prefrontal cortex (DLPFC) based on
157 sgACC-related functional connectivity (FC) is crucial for developing effective depression
158 treatments [6,7]. In light of inconsistent findings derived from studies with small sample sizes
159 [8-14], we set out to establish a large sample to identify a reliable abnormal sgACC-DLPFC FC
160 profile in MDD and further integrate this profile with individual brain activity to generate
161 individualized neuromodulation targets for treating depression.
162
163 Numerous investigations have delved into FC abnormalities in MDD using resting-state
164 functional magnetic resonance imaging (R-fMRI). Abnormal FCs between sgACC and
165 amygdala, thalamus, temporal gyrus, lingual gyrus, cerebellum, DLPFC, and default mode
166 network (DMN) regions such as medial and dorsal medial prefrontal cortex, precuneus, and
167 parahippocampus have been reported [8,9,12-19]. However, findings have been inconsistent,
168 making integrating findings and generating precise profiles of sgACC-related FC abnormalities
169 challenging. This deficiency in reproducibility could be partially due to small sample sizes and
170 low statistical power of clinical imaging studies [20,21]. To address the issue of limited sample
171 size, we initiated the Depression Imaging REsearch ConsorTium (DIRECT) [22] and conducted an
172 initial meta/mega-analysis (N_{MDD} = 1300), referred to as REST-meta-MDD [23]. DIRECT Phase I
173 shared ROI-level signals, thus enabling the investigation of multiple MDD-related
174 abnormalities in network FC, FC topological and dynamic features, and functional
175 lateralization [23-30]. In DIRECT Phase II data reporting, we pooled an expanded MDD sample
176 (N_{MDD} = 1660), which was preprocessed with a surface-based pipeline, DPABISurf [31]. DIRECT

177 Phase II shared voxel/vertex level BOLD time series, allowing more flexible and thorough
178 investigations. Leveraging the most comprehensive MDD R-fMRI dataset to date
179 encompassing depression patients and healthy controls, we can determine an aberrant
180 sgACC-FC profile associated with depression, characterized by superior reproducibility and
181 low risk of false positives.
182
183 Maps of sgACC-related FC abnormalities are clinically useful for predicting repetitive
184 transcranial magnetic stimulation (rTMS) treatment outcomes in MDD patients [32-34].
185 Specifically, the anticorrelation between sgACC and left DLPFC has been associated with
186 clinical improvement from rTMS treatment [35-39]. This has led to the intriguing notion that the
187 FC between sgACC and left DLPFC could be leveraged to identify more precise rTMS targets
188 and improve the efficacy of rTMS delivered to the left DLPFC [6,40]. Researchers have identified
189 a group-wise TMS target [37], which was the most anticorrelated DLPFC site to sgACC in the
190 mean FC map from a large cohort of healthy adults. Subtle but significant case-control
191 differences in resting-state FC profiles have been identified in a large sample of MDD
192 patients[23]. Thus, understanding the profiles of sgACC FC case-control differences and their
193 impact on potential targets for rTMS applied to the left DLPFC could be a critical step toward
194 developing optimized rTMS target site identification methods.
195
196 Individual human brains exhibit highly heterogeneous functional organization [41], with the
197 DLPFC regions exhibiting the highest level of interindividual variation in cytoarchitecture,
198 brain function, and network connectivity profiles [7,42]. While several individualized FC-guided
199 TMS target identification algorithms have been proposed [35,40,43-47], the target localizations of
200 most existing TMS protocols have not been individualized. The major obstacles to identifying
201 individualized TMS locations are the low signal-to-noise ratio in the sgACC area and the poor
202 reproducibility of individual FC maps [48,49]. The high reliability and statistical power of the
203 DIRECT MDD cohort (N_{MDD} = 1660) allow the integration of group-level statistical maps and
204 individual functional brain images to achieve precise and reliable TMS localization. Here, we
205 propose an algorithm based on dual regression (DR), which was initially developed for

206 mapping group-level independent component analysis (ICA) results onto individual brains [50].
207 Utilizing the DR-based algorithm avoids calculating FC based on the individual level time
208 series of a noisy area such as the sgACC. The computation of this algorithm was based on DR
209 of fMRI signals from the DLPFC region, which has a higher signal-to-noise ratio compared to
210 the sgACC. Thus, this algorithm enhances the efficacy and reliability of individualization
211 approaches for identifying TMS targets [51].
212
213 In the present study, we leverage a large-scale multi-center sample (DIRECT Phase II, 1660
214 MDD patients and 1341 healthy controls (HCs)) to derive a reliable sgACC-related FC
215 abnormality profile for MDD. We aimed to assess the role of the sgACC-related FC in the
216 precise localization of TMS targets. To facilitate individualized localization, we aimed to
217 develop a DR-based targeting algorithm that significantly enhanced the correlation between
218 target position and the reduction of clinical symptoms. We hypothesized that MDD patients
219 will show a significantly abnormal sgACC-FC profile, especially in the left DLPFC. We also
220 hypothesized that our newly-developed DR-based algorithm will outperform traditional TMS
221 group targets. To our knowledge, this is the first study to utilize a dual regression algorithm
222 to integrate large-scale group-level statistical maps with individual-level spontaneous brain
223 activity to achieve individualized TMS targeting in MDD.
224

225 Materials and methods

226 Study sample

227 This study utilized three independent datasets. The first dataset ("DIRECT") is a large-scale,
228 multi-sited consortium sharing standardized preprocessed R-fMRI time series. Building on
229 the initial success of DIRECT Phase I, consortium members and international collaborators
230 met on May 11th-12th, 2019, and agreed to launch DIRECT Phase II, which comprises 23
231 case-control designed datasets, including R-fMRI and T1 structural scans from 1660 MDD
232 patients and 1341 HCs. Researchers from each site later took a 2-day DPABISurf training

course on September 14th-15th, 2019, to harmonize the organization and preprocessing of R-fMRI/T1 structural data. Demographic and clinical characteristics for each sample are presented in Figure 1 and Table 1. Site information, sample size, and previous publications based on the shared data are listed in Table S1. All participants were asked to self-report their sex (biological attribute) as part of the case report form (CRF). All participants in DIRECT Phase II were East Asian. Patients were diagnosed with MDD based on ICD 10 or DSM-IV. Healthy controls who were matched with MDD patients by age, sex ratio, and educational levels were recruited at each site. All participants provided written informed consent, and local institutional review boards approved each study from all included cohorts. The analysis plan of the current study has been reviewed and approved by the Institutional Review Board of Institute of Psychology, Chinese Academy of Sciences (No. H21102). Data will be made available to the public as outlined in the Data Sharing Statement.

The second dataset ("TRD-TMS") comprises 25 medication-treatment-resistant MDD (TRD) patients who underwent 4 to 7 weeks of daily repetitive TMS applied over the left DLPFC. Patients' TMS sites were recorded using their structural MRI images and a frameless neuronavigation system. Treatment response was assessed with the 24-item Hamilton Depression Rating Scale (HAMD). Only TMS outcomes and target coordinates were openly shared for this dataset. We get access to these data from the supplementary materials of Weigand et al. [37] For more details on this dataset, please refer to Weigand et al. [37]

The third dataset ("CUD-TMS") comprises 27 cocaine use disorder (CUD) patients who underwent two daily sessions of rTMS treatment over the left DLPFC in an acute phase and two weekly sessions of rTMS treatment in a maintenance phase. The TMS outcomes, neuroimaging data, participants' demographic info, and target coordinates for this dataset were openly shared. Depressive symptoms were a secondary treatment outcome in the original study and were used to validate the localization algorithm's clinical relevance in the current study. In addition, this dataset shared participants' baseline R-fMRI data (https://openneuro.org/datasets/ds003037/versions/1.0.0), which allowed for the

calculation of individualized optimal TMS targets. For more details on this dataset, see Garza-Villarreal et al. [52]

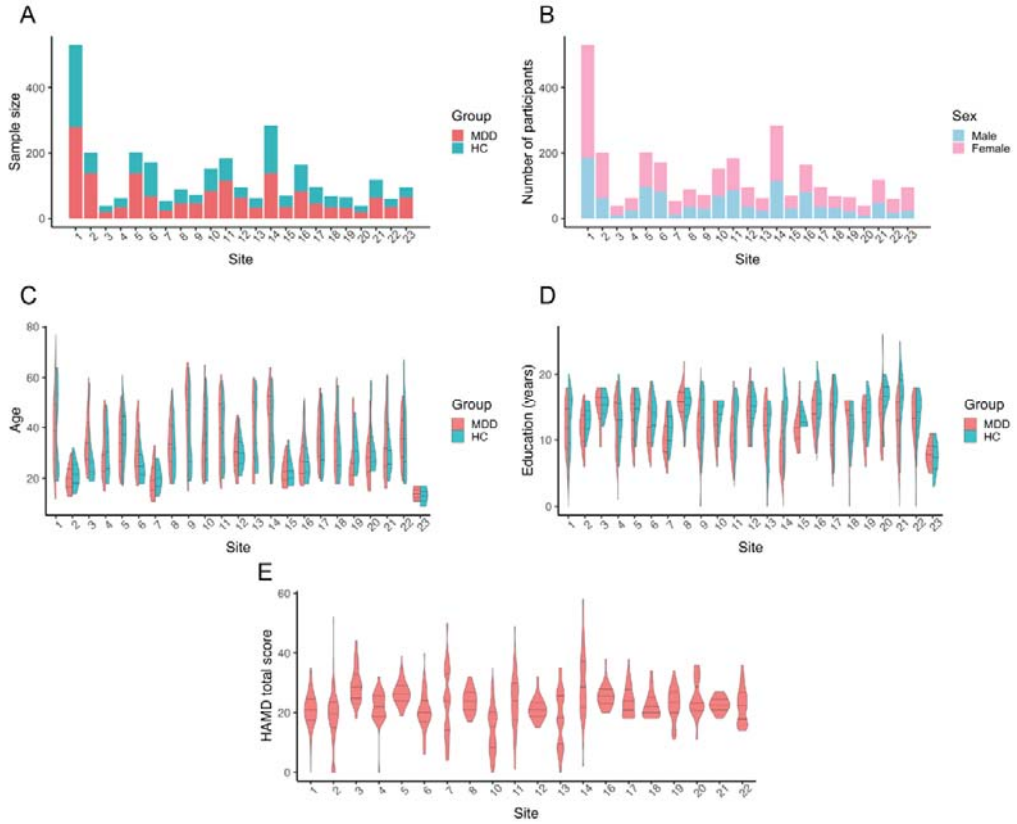

Figure 1. Sample characteristics of the DIRECT dataset. (A) Sample sizes of each site; (B) Number of male/female subjects irrespective of diagnosis; (C) Violin plots depicting the age distribution (in years). Solid black lines indicate the mean, 25th, and 75th percentiles; (D) Violin plots show education distribution (in years). Solid black lines indicate the mean, 25th, and 75th percentiles; (E) Violin plots depicting the distribution of scores of the Hamilton Depression Rating Scale (HAMD). Solid black lines indicate the mean, 25th, and 75th percentiles.

Approach

The study's first objective was to delineate case-control differences in sgACC-FC profile and explore its implication in identifying FC-guided individualized TMS targets. Accordingly, we

275 conducted a generalized linear model (GLM) to compare voxel-wise sgACC-FC maps of MDD
276 patients and HCs in the DIRECT dataset. We then demonstrated the association between
277 clinical improvement and group differences in TMS targeting sgACC-FCs by leveraging the
278 TRD-TMS dataset. Given that the peak sgACC anticorrelation of a normative connectome
279 within the left DLPFC was usually selected as the FC-guided sgACC group target, we showed
280 the impact of case-control differences on such group targets by separately identifying the
281 peak sgACC anticorrelation in the mean sgACC-FC maps of the MDD group and HC group
282 from the DIRECT dataset. Finally, we identified individualized optimal targets using a
283 DR-based algorithm guided by statistical maps (e.g., group difference map, mean sgACC-FC
284 maps). We validated the clinical effectiveness of the individualized approach by computing
285 the correlation between clinical outcome and the distance between the actual TMS sites and
286 the identified individualized targets in the CUD-TMS dataset. All statistical tests conducted in
287 the current study were two-sided.

288 **Power calculations for primary hypothses**

289 The primary outcome of the current study is the case-control differences regarding the
290 sgACC-FC profiles. Estimates of the effect size (Cohen's d = 0.186) of MDD patients'
291 abnormalities in FCs draw directly from our prior research based on the DIRECT Phase I
292 dataset [23]. Power calculation was performed using R version 4.3.1 [53] with pwr [54]. A sample of
293 455 patients will achieve 80% power with a 5% Type I error rate.

294 **Image preprocessing**

295 Acquisition parameters and scanners for all cohorts are provided in Table S2. All R-fMRI and
296 structural MRI scans were preprocessed at each site using the same DPABISurf protocol, an
297 R-fMRI data analysis toolbox evolved from DPABI/DPARSF [31,55,56] (For details, see SI). Given
298 the controversy regarding global signal regression (GSR) and its essential role in identifying
299 TMS targets [40], we performed preprocessing pipelines with and without GSR.

300 **FC maps of sgACC**

301 Although recent studies have attempted to identify personalized TMS targets using
302 surface-based algorithms [43], most previous studies have reported targets in volume-based
303 MNI space with sgACC ROIs defined as a sphere in volume-based space [35,57]. To better
304 compare our results with the existing literature, we used the volume-based preprocessed
305 imaging data from DPABISurf.
306
307 We defined the sgACC as a 10 mm diameter sphere located on the average MNI coordinates
308 based on prior studies showing reduced glucose metabolism or blood flow after receiving an
309 antidepressant treatment (MNI coordinates: x = 6, y = 16, z = -10. For details, please refer to
310 Fox et al., 2012 [35]). The sgACC time series were determined for each individual by spatially
311 averaging the preprocessed R-fMRI time series across all voxels in the abovementioned
312 masks. We then calculated whole-brain FC maps in volume-based MNI space. FC was
313 calculated using Pearson's correlation and underwent Fisher's r-to-z transformation. All FC
314 maps were smoothed with a 6 mm full-width half maximum (FWHM) kernel size. We used
315 ComBat [58] to control potential site and scanner biases (For details, see SI).

316 **Group difference maps of sgACC-FC profiles**

317 We used a voxel-wise GLM to examine differences in the FC maps of sgACC between MDD
318 patients and HCs in DIRECT Phase II. Cohen's f^2 was calculated to characterize the effect sizes
319 of this group difference effect. The GLM model includes age, sex, education, and head
320 motion as covariates:

321 $$\boldsymbol{y} = \boldsymbol{\mu} + \boldsymbol{X\beta} + \boldsymbol{\epsilon} \quad (1)$$

322 where y denotes the FC value of a given voxel from a given participant; $\boldsymbol{\mu}$ stands for the
323 constant term; X represents the design matrix for the covariates of interest (diagnosis, age,
324 sex, education, and head motion); $\boldsymbol{\beta}$ is a vector of regression coefficients corresponding to X;
325 and $\boldsymbol{\epsilon}$ is a vector of residuals that follow $N(0, \boldsymbol{\sigma}^2)$. Multiple comparison correction was
326 conducted using false discovery rate (FDR) correction at $q < 0.05$.

327 **Relationship between group differences in TMS targets' sgACC FCs and clinical outcomes**

328 To explore the relationship between group differences in TMS targets' sgACC FCs and clinical
329 outcomes, we first extracted the mean *t*-values from the group difference map of 4 mm
330 radius spheres centered at each targeting coordinate in the TRD-TMS dataset, then examined
331 the Pearson correlations between these *t*-values and HAMD score reductions. We
332 anticipated that greater group differences in sgACC-FC at the target location (i.e., higher *t*
333 values), would be related to better TMS therapeutic effect (higher HAMD reductions).

334 **Group targets based on mean sgACC-FC maps**

335 The prior group-level DLPFC TMS target had been derived from a cohort of healthy young
336 adults [37]; here, we averaged whole-brain sgACC-FC maps across all the DIRECT participants in
337 the MDD and HC groups separately. We then searched for the peak sgACC anticorrelated
338 voxel within the DLPFC area (i.e., Brodmann area (BA) 46) as the mean sgACC-FC guided TMS
339 targets for the MDD and HC groups.

340 **Identification of individualized TMS targets by dual regression**

341 Given the greater reliability of statistical maps from a large cohort of subjects (N_{MDD} = 1660 in
342 the DIRECT dataset), we used DR to identify individualized TMS targets guided by group-level
343 statistical maps (Figure 2).
344
345 We used a two-step algorithm to back-reconstruct the corresponding subject-specific spatial
346 patterns based on group-level components [50] (see Figure S4 for details). First, an
347 individual-level time course measuring how the group-level template fitted into the brain
348 BOLD signal spatial pattern at every time point was calculated using least-squares for each
349 participant. We used three group-level sgACC FC statistical maps (i.e., the group difference
350 map, the mean MDD sgACC-FC map, and the mean HC sgACC-FC map) as group templates in
351 the DR-based algorithm. As the two clusters that survived FDR correction ($q < 0.05$) were too
352 small to be used as group templates in the DR computation, we expanded them by applying

353 a more liberal multiple comparison correction threshold (FDR $q < 0.1$). In addition, we
354 reversed the mean MDD/HC sgACC-FC maps to generate the most sgACC-anticorrelated brain
355 area in DLPFC before conducting regressions. Second, the time course derived in the first
356 step was used as a temporal regressor to estimate subject-specific spatial maps. The
357 subject-specific maps were considered the best approximation of the group-level template
358 for single participants. This benefits from the group-level prior information based on a large
359 sample and the subject-specific spontaneous brain activity. The center of mass of the largest
360 cluster in the subject-specific maps was calculated to determine the final TMS targeting
361 coordinates. These clusters were extracted from the thresholded subject-specific maps in
362 which only the top-*n* voxels in the DLPFC mask were retained. The thresholds were related to
363 the type and size of the group template input into the DR algorithm and incrementally varied
364 between 5 and 100 voxels. The threshold for the DR approach guided by the FDR-corrected
365 group difference map was set to 10, and the threshold for the DR approach guided by mean
366 sgACC-FC maps was set to 50 voxels (Figure S5). We chose BA 46 as the DLPFC mask in the DR
367 approach because prior studies have reported that BA 46 is more anticorrelated to sgACC
368 than alternative DLPFC definitions[35] (e.g., BA 9, Beam F3, or the 5 cm method) and suggested
369 that a more anterior and lateral location was related to better treatment response in MDD
370 TMS treatment [7,37].

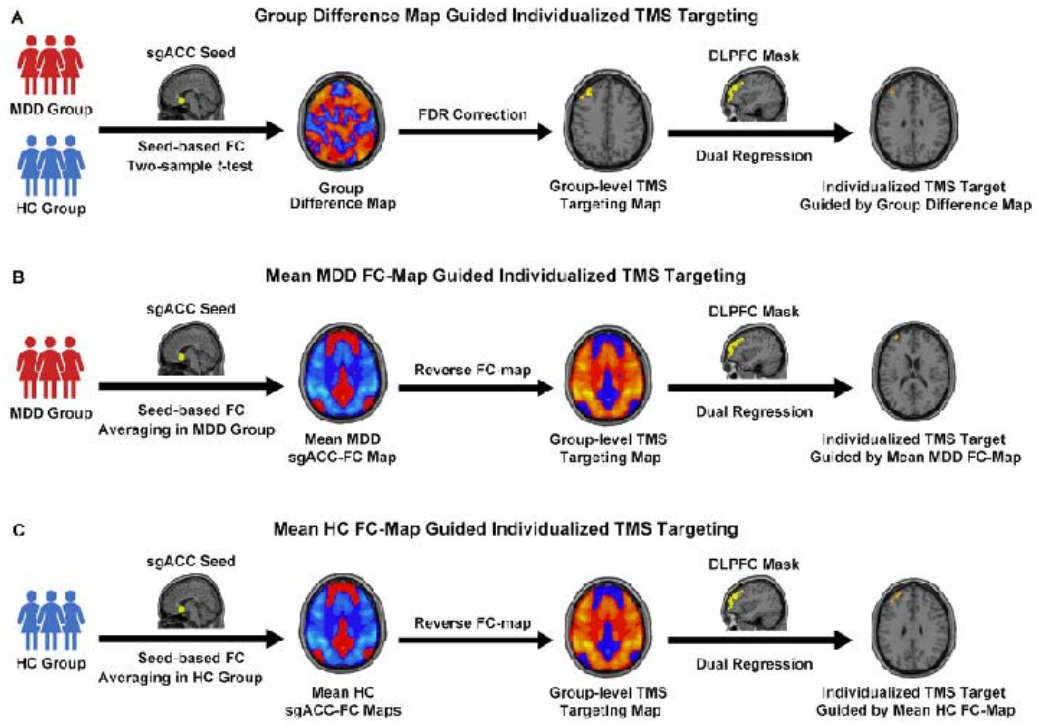

Figure 2. Schematic diagram of the statistical map guided individualized rTMS targeting algorithms. (A) The sgACC-FC group difference map guided individualized target localization. (B) The mean MDD sgACC-FC map guided individualized precise target localization. (C) The mean HC sgACC-FC map guided individualized precise target localization.

Clinical effectiveness of the group-level and individualized TMS targets

We leveraged the CUD-TMS dataset to evaluate the clinical significance of individualized TMS targets. In the CUD-TMS dataset, rTMS was delivered at the left DLPFC using either the 5.5 cm anatomic criterion or the Beam F3 method. We selected participants with a baseline HAMD score greater than 7, yielding a subsample of 16 individuals, and calculated their maximum HAMD reductions during the entire treatment course as an index of TMS therapeutic efficacy. We identified the proposed DR-based individualized TMS targets guided by the group difference map or the mean sgACC-FC maps and calculated the targeting offset (i.e., Euclidean distance between the individualized optimal TMS targets and the actual stimulation coordinates) for each patient. Subsequently, we calculated the Pearson

correlations between clinical improvement (i.e., HAMD reductions) and targeting offset. We anticipated a negative correlation between clinical outcomes and target offset (i.e., the closer the actual stimulation target was to the individualized DR-based target, the higher the clinical improvement). Age, sex, education, and head motion were included as covariates in the regression models when calculating correlations between targeting offsets and clinical improvement.

Results

Group difference maps of sgACC-FC

In the large-scale DIRECT dataset, we found significant MDD-related hyperconnectivity with the sgACC in bilateral DLPFC, temporal parietal junction, and occipital lobe, as well as hypoconnectivity in the bilateral temporal lobe, left inferior frontal gyrus, and left postcentral gyrus when preprocessing included GSR (Figure 3A). When GSR was not included in preprocessing, MDD-related sgACC FC alterations showed predominantly hypoconnectivity. Such abnormally decreased FCs were found across the central gyrus, occipital lobe, insular cortex, temporal lobe, and a small portion of the frontal lobe. Without GSR, MDD-related hyperconnectivity was limited to subcortical regions (Figure S1). Given that significant case-control differences in the DLPFC area were revealed only when GSR was implemented, subsequent analyses were solely based on results with GSR. We thus identified two contiguous clusters of voxels that showed significant group differences in the left DLPFC. Group difference cluster 1 (MNI coordinates: x = -44, y = 38, z = 32; $t(2880) = 3.277$, $p < 0.001$, Cohen's $f^2 = 0.004$) was ventral to group difference cluster 2 (MNI coordinates: x = -34, y = 36, z = 40; $t(2880) = 3.670$, $p < 0.001$, Cohen's $f^2 = 0.005$) (Figure 3B).

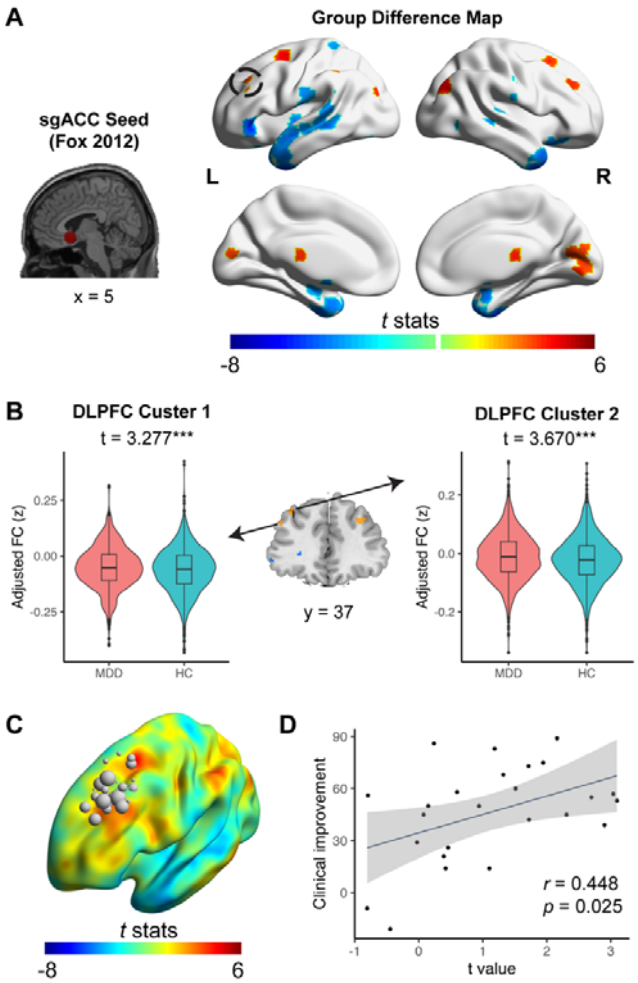

Figure 3. Group differences of subgenual anterior cingulate cortex (sgACC) functional connectivity (FC) profiles are related to TMS treatment efficacy, demonstrating clinical significance. (A) Two-sample *t*-test maps of MDD-related sgACC FC abnormalities with global signal regression (GSR) implemented. (B) Two clusters showed significant case-control differences in sgACC-FC. (C) The TMS targets were extracted from the TRD-TMS dataset [37]. The sizes of the spheres indicate the magnitudes in Hamilton Depression Rating Scale (HAMD) reductions, with the group difference map rendered on the surface. (D) The magnitudes of the group differences in the FC between TMS targets and sgACC were positively related to clinical improvements in the TRD dataset.

sgACC-FC group differences correlate with TMS treatment outcomes

Using the TRD dataset, we examined the relationship between group differences (*t*-values)

422 and clinical outcomes (HAMD reductions) to test the clinical relevance of the group
423 difference maps. Group differences were positively correlated with HAMD score reductions
424 ($r(23) = 0.448$, $p = 0.025$, Figure 3C-D), suggesting that group-level difference maps may be
425 useful for enhancing the outcomes of TMS for treating MDD by improving target localization.

426 **sgACC anticorrelation peaks in MDD and HCs**

427 Our results highlighted the case-control differences in sgACC-FC profiles. Since the prior
428 sgACC group target (MNI coordinates: x = −42, y = 44, z = 30) had been based on a cohort of
429 young, healthy adults [37], we sought to examine potential differences in anticorrelation peaks
430 extracted from the mean sgACC FC maps of MDD and HC groups (Figure 4B-C) in the DIRECT
431 dataset. We found that the anticorrelation peak of MDD patients (MNI coordinates: x = -40, y
432 = 50, z = 22) differed from that of HCs (MNI coordinates: x = -42, y = 38, z = 32), probably due
433 to abnormal FCs within the left DLPFC in MDD patients. The anticorrelation peak extracted
434 from the DIRECT HCs was closer to the previously reported locus [37] (Figure 4).

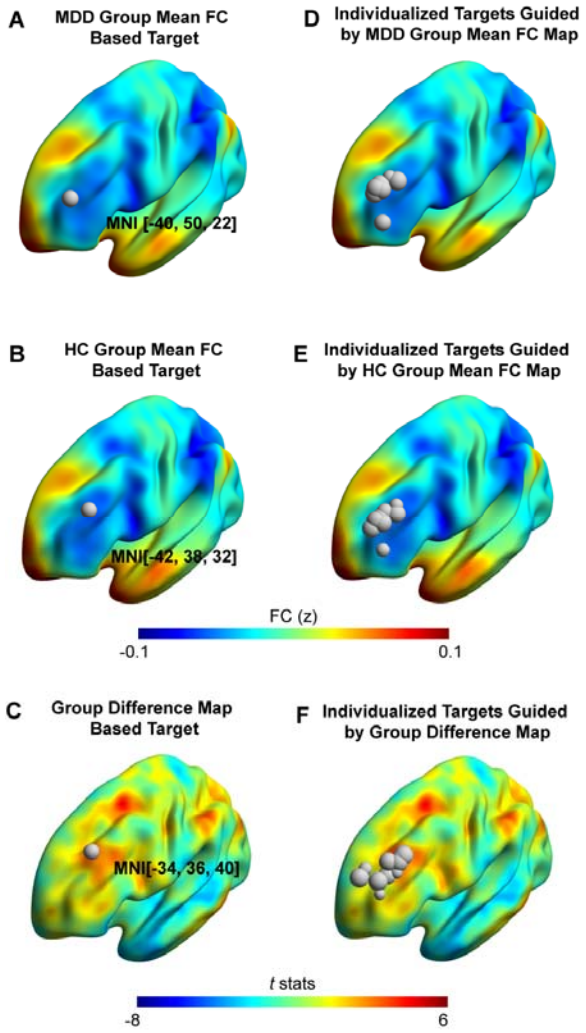

Figure 4. Distribution of dual regression (DR) based individualized TMS targets guided by different subgenual anterior cingulate cortex (sgACC)-FC statistical maps. The peak of the sgACC anticorrelation in MDD patients differed from that in HCs. (A) The peak sgACC anticorrelation location in the average sgACC-FC map of the MDD group in the DIRECT dataset. (B) The peak sgACC anticorrelation location in the average sgACC-FC map of the HC group in the DIRECT dataset. (C) The sgACC-FC case-control group difference map and the peak in the left dorsal lateral prefrontal cortex (DLPFC) in the DIRECT dataset. (D-F) DR-based individualized TMS targets guided by the mean HC sgACC-FC map, the mean MDD sgACC-FC map, and the group difference map, respectively. The sizes of the spheres indicate the magnitudes of Hamilton Depression Rating Scale (HAMD) reductions.

Individualized targets suggest higher clinical efficacy than group targets

To integrate the reliable group-level statistical map information based on large samples with individual spontaneous brain activity, we utilized a DR-based approach to calculate individualized optimal targets for each participant based on three group-level statistic maps. The individualized target locations are illustrated in Figure 4. The clinical relevance of the targets was determined by the correlation between target offset and clinical improvement in the CUD dataset. All the individualized targets (Figure 5D-F) outperformed their corresponding group-level targets (Figure 5A-C). Among the three individualized targets, the targets based on group-level difference maps ($r(14) = -0.560$, $p = 0.029$) outperformed the individualized targets based on the MDD group-average template ($r(14) = -0.375$, $p = 0.115$) or the HC group-average template ($r(14) = -0.372$, $p = 0.117$).

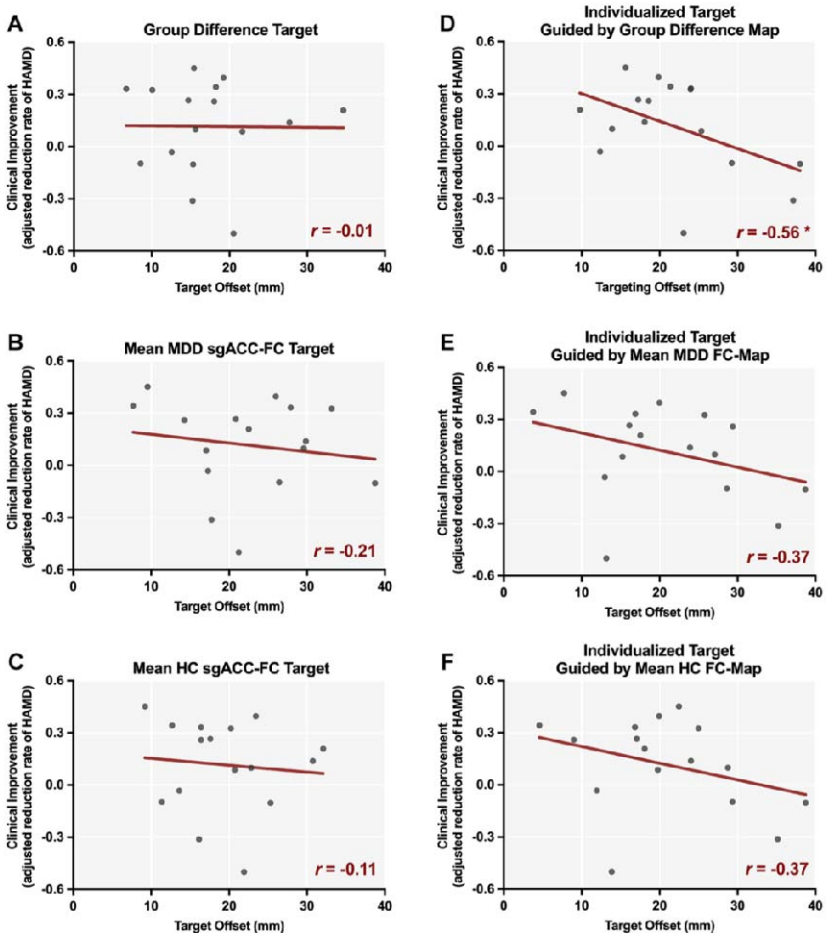

Figure 5. The individualized targets exhibited greater clinical efficacy compared to the group targets.

459 Clinical efficacy was characterized by computing the correlations between the offset distances of TMS
460 targets and the clinical improvements observed in the CUD-TMS dataset. The TMS targeting offset
461 distance was defined as the Euclidean distance between the actual rTMS stimulation coordinates and
462 the group/individualized targets. Clinical improvement was defined as the maximum HAMD reduction
463 during rTMS treatment, adjusted for age, sex, education, and head motion. (A-C) The clinical efficacy
464 of the group targets. (D-F) The clinical efficacy of the individualized targets. *$p < 0.05$.
465

466 **Discussion**

467 In the present study, we leveraged a large multi-site fMRI sample (1660 MDD patients and
468 1341 HCs) and two openly shared TMS datasets to delineate abnormalities in sgACC FC in
469 MDD and explore their potential impact on the localization of TMS targets. Specifically, with
470 GSR implemented, we found enhanced FCs between sgACC and left DLPFC, bilateral
471 supplementary motor areas and inferior parietal lobes, thalamus and visual areas, and
472 decreased FCs between sgACC and left anterior insula, left superior temporal lobe, and
473 bilateral temporal poles in MDD patients. Crucially, we showed that the clinical outcomes of
474 TMS treatments were related to the magnitude of the case-control differences in the FCs
475 between sgACC and TMS targets. Furthermore, the thresholded group difference maps
476 showed outstanding performance when identifying individualized TMS targets. Additionally,
477 the DR-based approach to identify individualized TMS targets showed better clinical efficacy
478 than TMS targets based on group sgACC-FC profiles.

479 **MDD-related FC abnormalities of sgACC**

480 Our results add to a growing literature documenting functional network abnormalities
481 involving the sgACC in MDD[8,10-12,16,18,59-61]. Nevertheless, notable discrepancies in the type of
482 abnormality (enhanced/reduced) and specific brain regions showing altered sgACC FCs have
483 been reported. Considering the small effect sizes (Cohen's $f^2 < 0.01$) of MDD-related
484 sgACC-FC abnormalities, the limited sample sizes in previous studies entail a high risk of false
485 positive findings [20,62,63]. Another potential source of heterogeneity in previous findings may
486 be whether or not they applied GSR (See the supplementary materials for detailed

487 discussion). With an unprecedented sample size, our results provide among the most robust
488 evidence to date. Specifically, MDD patients showed enhanced sgACC-thalamus FC and
489 decreased sgACC-limbic network FC regardless of whether GSR was implemented. These
490 results are consistent with previous studies in adolescents [18] and adults [57] with MDD.
491 Previous studies have reported abnormal FCs between sgACC and limbic areas and some
492 subcortical regions, such as the amygdala [8,19] and parahippocampus regions [12]. Together,
493 these results are consistent with a model highlighting sgACC as a critical hub in an "extended
494 medial network," which also encompasses limbic, thalamic, and striatal regions and plays a
495 key role in the pathophysiology of MDD [64,65]. This "extended medial network" overlaps
496 substantially with the DMN. Indeed, decreased FCs between sgACC and DMN regions, such
497 as the medial prefrontal cortex, precuneus, temporal gyrus, and parahippocampus regions,
498 were revealed in MDD relative to HCs when GSR was not implemented. Such abnormalities
499 have been previously reported [9,11,14,33], which led to the hypothesis that abnormally
500 enhanced FC between sgACC and DMN are the network underpinnings of rumination [66].
501 However, contrary to the aforementioned hypothesis, we found reduced, instead of
502 enhanced FC between sgACC and DMN. Similarly, in the first phase of DIRECT, we
503 demonstrated that MDD was characterized by reduced FC within DMN [22,23]. We note that
504 both the first phase and the current second phase of the DIRECT data are solely comprised of
505 Chinese samples, while most studies that have reported enhanced sgACC-DMN FCs have
506 been in Caucasian samples. Different prevalence rates [67,68], heterogeneous symptoms [69], and
507 different risk alleles [70] have been reported in Caucasian and Eastern Asian groups.
508 Accordingly, we cannot exclude racial differences contributing to this discrepancy.

509 **Clinical relevance of abnormal sgACC-DLPFC anticorrelation in MDD**

510 Once the group difference maps of sgACC FC profiles were delineated, we further explored
511 the impact of such an abnormality, especially in DLPFC, on identifying TMS targets. Most
512 clinical trials have focused on applying TMS to the left DLPFC based on the hypothesis that
513 high-frequency rTMS will enhance hypoactivity during depressive episodes [7,71]. The DLPFC is
514 anatomically extensive, comprising BA 46 and BA 9 [72]. However, which DLPFC sub-field is the

515 best target for TMS remains unclear. The current FDA-approved protocol (i.e., the "5 cm"
516 method) leads to large interindividual variation in stimulation sites, which may contribute to
517 the heterogeneity in the effect sizes of antidepressant responses in prior trials [73,74].
518
519 However, leveraging anatomical landmarks to target the boundary between BA 9 and BA 46
520 precisely has not consistently outperformed the "5 cm" method or the F3 Beam method [75,76].
521 Considering the unsatisfactory effect of TMS target localization based on brain anatomical
522 parcellation, group-level normative sgACC anticorrelation peaks based on healthy population
523 datasets have been frequently used as TMS targets in recent years [35,37,40]. However, in the
524 present study, we found that the locations of such anticorrelated peaks differ substantially
525 between MDD and HC samples when measured in a large clinical cohort. Therefore, it might
526 be problematic to identify TMS targets based solely on sgACC-FC profiles in healthy or
527 depressed individuals. Intriguingly, we found that the magnitudes of case-control differences
528 in TMS targets' FCs to sgACC were positively related to the clinical improvements after
529 receiving rTMS to the left DLPFC. Such correlation implies that the case-control differences in
530 the FC between sgACC and the left DLPFC might bear important information that could be
531 leveraged to guide the identification of reliable, individualized TMS targets.

532 **A DR-based individualized approach may improve the clinical efficacy of TMS targets**

533 In the current study, we developed a DR-based approach to individualize the TMS targets
534 derived from group-level statistical maps. The proposed approach takes advantage of the
535 high signal-to-noise ratio and reliability of large sample statistical maps while integrating
536 individual spontaneous brain activity of individuals with MDD. Most existing individualized
537 TMS target localization algorithms are based on calculating sgACC FCs using densely sampled
538 MRI images from single subjects [77]. However, individual MRI images tend to be noisy and
539 unreliable [78,79], especially in the sgACC region. Air in the sinuses often introduces
540 susceptibility artifacts due to the different magnetic properties of air and brain tissue. Signal
541 loss and geometric distortion are common in areas close to air-filled sinuses, such as the
542 inferior frontal cortex, including the sgACC [80]. The seed map approach has been proposed to

543 alleviate such difficulties due to the subpar image quality of the sgACC region [40,43].
544 Nevertheless, the sgACC is still the major contributor to the seed time series extracted for
545 the seed map, and the final targeting approach still relies on calculating FC using MRI images
546 from a single subject. A cutting-edge MDD TMS therapy combining FC-guided target
547 localization, high dose, and intermittent theta-burst stimulation (iTBS) was reported to be
548 highly effective in a randomized, double-blinded, sham-controlled clinical trial [44,45]. However,
549 the targeting algorithm relied on hierarchical agglomerative clustering in the sgACC area
550 which has a low signal-to-noise ratio. However, the final target was still determined
551 according to individual-level sgACC-DLPFC FCs. For the proposed DR-based approach, the
552 entire regression computation procedure at the individual level is conducted in the DLPFC
553 region, which is less affected by susceptibility artifacts. In this way, the superior signal quality
554 of DLPFC and the effective and reliable properties of the dual regression algorithm enhance
555 the accuracy of target localization.
556
557 Encouragingly, the DR-based individualization targets enhanced the clinical significance of
558 corresponding group-level targets, regardless of which template was used. This result
559 supports the generalizability and extensibility of the algorithm, offering the potential for TMS
560 targeting based on other circuits and biomarkers. Considering the majority of existing TMS
561 research still relies on the traditional 5 cm or Beam F3 methods for targeting, one approach
562 based on our data to improve targeting would be to simply shift the target to a more anterior
563 and lateral position. However, such a simple shift was not supported by the present study.
564 Instead, 25% of targets individualized using the group difference map were more medial than
565 the original targets, and 50% of targets individualized by the group difference map were
566 more posterior than the original targets. Therefore, the DR-based algorithm does not simply
567 set a more anterior and lateral coordinate in the BA46 area as the individualized optimization
568 target for subjects. Among the group-level templates used in the DR-based individualized
569 algorithm, the sgACC-FC group difference map performed the best, instead of the commonly
570 used average sgACC based on healthy individuals. This may reflect the abnormal posterior
571 shift of the MDD sgACC anticorrelation peak we found, and it emphasizes the immense

572 clinical value of examining spontaneous brain activity differences between MDD and HC in a
573 large sample. Previous studies either included only a small quantity of MDD functional MRI
574 data [45,46,81] or developed targeting algorithms based on large-scale HC samples [48]. In this
575 paper, we utilized an unprecedented amount of functional MRI data from both MDD and HC,
576 obtained a reliable group-level difference map of sgACC-FC, and successfully validated its
577 potential in treating MDD with TMS.
578

579 **Limitations**

580 Several limitations need to be considered. First, we noted that the inconsistency between
581 our results and the broader literature could partly be due to racial differences of the samples
582 (i.e., Eastern Asian vs. Caucasian). Consortiums that intend to pool existing neuroimaging
583 data worldwide, such as the Enhancing NeuroImaging Genetics through Meta-Analysis
584 (ENIGMA) Major Depressive Disorder (MDD) consortium [24], have accumulated large-scale
585 data primarily from Western countries and published several high-impact studies delineating
586 MDD-related anatomical abnormalities [82,83]. Planned collaborations between the DIRECT and
587 the ENIGMA-MDD consortiums may help address potential cultural, genetic, and
588 environmental mechanisms in more diverse groups of MDD patients. Second, we performed
589 volume-based preprocessing to facilitate comparison with previous literature. Surface-based
590 preprocessing strategies have provided more accurate and detailed representations of
591 cortical and subcortical structures [84]. Recent research has begun to explore surface-based
592 rTMS target identification algorithms and has shown promising clinical relevance [38,39,85].
593 Future research should consider using surface-based case-control difference maps to further
594 refine ways to identify TMS targets. Given the established involvement of the left DLPFC in
595 the existing TMS treatment protocols, the present study restricted the investigation within
596 this area. We noted that other brain regions (e.g., angular gyrus and supplementary motor
597 area) showing significant case-control differences worth further research and may serve as
598 potential targets for neuromodulation [86,87].
599

600 Identifying a reliable personalized TMS target solely based on an individual's R-fMRI data
601 (around 8 mins of fMRI scan in clinical practice) is challenging. Due to the poor replicability of
602 FC [88], existing individual-level network parcellation algorithms need a large quantity of fMRI
603 images (usually more than one hour of scanning time)[89]. The present study utilized two
604 openly-shared TMS samples to validate the efficacy of the individualized algorithm. However,
605 prospective, double-blind clinical trials are warranted to compare the treatment outcome
606 across different rTMS targeting algorithms (e.g., traditional anatomical landmark-based
607 targeting, group-level sgACC-FC targeting, and DR-based individualized targeting methods).
608 In addition, mounting evidence has suggested that MDD patients may benefit from rTMS
609 over alternative targets such as dorsomedial prefrontal cortex (DMPFC) [90]. The DR-based
610 individualized positioning algorithm can be readily transferred to other neural circuits or
611 other brain imaging-derived feature maps (e.g., ICA, functional gradient, normative
612 modeling). The clinical efficacy of these alternative targets is worthy of future investigations.
613

614 **Conclusion**

615 In summary, we leveraged a large sample of MDD patients to fully delineate group
616 differences in sgACC-FC maps between MDD patients and HCs. We next demonstrated the
617 impact of such case-control differences on group TMS targets based on sgACC-FC profiles by
618 showing that the magnitudes of case-control differences in the FC between sgACC and TMS
619 targets were positively associated with clinical outcomes. The peak sgACC anticorrelation
620 locations were different in MDD patients as compared to HCs. Moreover, we developed a
621 DR-based approach to identify individualized TMS targets and demonstrated that this
622 approach may improved clinical efficacy compared to group targets based on sgACC-FC
623 profiles.

624 **Contributors**

625 C-GY, Y-FZ, X-NZ, XC, and BL conceived and designed the study. C-GY, Y-FZ, J-PZ, and X-NZ

626 coordinated the collaboration. JQ, LK, T-MS, TL, K-RZ, Z-NL, L-PC, JY, X-PW, Y-GY, C-YW, C-MX,
627 G-RX, Y-SL, Y-QY, XW, YW, X-FX, Y-QC, Q-YG, W-BG, J-PZ, YH, H-NW, B-JL, WZ, and J-PL
628 supervised data collection. X-RW, QH, Y-KW, HY, A-XZ, Y-CL, J-SC, P-FS, X-YL, FL, C-CH, X-LC,
629 F-NJ, J-JZ, X-LJ, G-MC, Z-SC, T-LC, X-XS, TC, B-JL, M-LY, Z-PX and BL organized the data. XC and
630 C-GY analyzed and interpreted the data. BL and C-GY designed the dual regression-based
631 TMS targeting algorithm. XC, BL, and C-GY drafted the manuscript. All authors revised the
632 manuscript for important intellectual content and approved the final submitted version. XC,
633 BL, and C-GY accessed and verified the data. XC, BL, and C-GY had full access to all the data in
634 the study. C-GY had final responsibility for the decision to submit for publication. All authors
635 were responsible for the final decision to submit for publication and have seen and approved
636 the manuscript.

637 **Conflict of interest**

638 DMB receives research support from the Canadian Institutes of Health Research (CIHR),
639 National Institutes of Health – US (NIH), Brain Canada Foundation, and the Temerty Family
640 through the CAMH Foundation and the Campbell Family Research Institute. He received
641 research support and in-kind equipment support for an investigator-initiated study from
642 Brainsway Ltd. and he was the site principal investigator for three sponsor-initiated studies
643 for Brainsway Ltd. He received in-kind equipment support from Magventure for
644 investigator-initiated studies. He received medication supplies for an investigator-initiated
645 trial from Indivior. He has participated in an advisory board for Janssen. He has participated
646 in an advisory board for Welcony Inc.

647 **Inclusion and Ethics**

648 Local researchers were included throughout the research process. Research protocols have
649 been approved by local ethics review committees. No potential risk was involved in the
650 current research and all local researchers have discussed and approved the research protocol.
651 All participants provided written informed consent, and local institutional review boards

approved each study from all included cohorts. The analysis plan of the current study has been reviewed and approved by the Institutional Review Board of Institute of Psychology, Chinese Academy of Sciences (No. H21102).

Data sharing

According to the success of the data sharing model of DIRECT Phase I data (REST-meta-MDD, http://rfmri.org/REST-meta-MDD), DIRECT Phase II data will also have 2 sharing stages. 1) Stage 1: coordinated sharing, upon the publication of this announcing manuscript. To reduce conflict of the researchers, the consortium will review and coordinate the proposals submitted by interested researchers. The interested researchers first send a letter of intent to rfmrilab@gmail.com. Then the consortium will send all the approved proposals to the applicant. The applicant should submit a new innovative proposal while avoiding conflict with approved proposals. This proposal would be reviewed and approved by the consortium if no conflict. Once approved, this proposal would enter the pool of approved proposals and prevent future conflict. 2) Stage 2: unrestricted sharing, after January 1, 2026. The researchers can perform any analyses of interest while not violating ethics. All codes have been made openly available (https://github.com/Chaogan-Yan/PaperScripts/tree/master/Chen_2023).

Acknowledgments

This work was funded by the Sci-Tech Innovation 2030 - Major Project of Brain Science and Brain-inspired Intelligence Technology (No. 2021ZD0200600), the National Key R&D Program of China (No. 2017YFC1309902), the National Natural Science Foundation of China (No. 82122035, No. 81671774 and No. 81630031), the 13th Five-year Informatization Plan of Chinese Academy of Sciences (No. XXH13505), the Key Research Program of the Chinese Academy of Sciences (No. ZDBS-SSW-JSC006), Beijing Nova Program of Science and Technology (No. Z191100001119104), the Scientific Foundation of Institute of Psychology, Chinese Academy of Sciences (No. E2CX4425YZ and No. Y9CX422005), the China

Postdoctoral Science Foundation (No. 2019M660847), the China National Postdoctoral Program for Innovative Talents (No. BX20200360), the Special Research Assistant Program of the Chinese Academy of Sciences (No. E2CX0624), and the Scientific Foundation of Institute of Psychology, Chinese Academy of Sciences (grant number: E2CX4425YZ). The support provided by China Scholarship Council (CSC, No. 202104910248) during a visit of Xiao Chen to the Centre for Addiction and Mental Health is acknowledged. In addition, we would like to acknowledge the valuable insights provided by Prof. B.T. Thomas Yeo, whose comments helped to shape our understanding of the data and refine our analysis.

References

1 Malhi, G. S. & Mann, J. J. Depression. *Lancet (London, England)* **392**, 2299-2312 (2018). https://doi.org:10.1016/s0140-6736(18)31948-2

2 Drevets, W. C., Price, J. L. & Furey, M. L. Brain structural and functional abnormalities in mood disorders: implications for neurocircuitry models of depression. *Brain structure & function* **213**, 93-118 (2008). https://doi.org:10.1007/s00429-008-0189-x

3 Mayberg, H. S. Modulating dysfunctional limbic-cortical circuits in depression: towards development of brain-based algorithms for diagnosis and optimised treatment. *British medical bulletin* **65**, 193-207 (2003).

4 Mayberg, H. S. *et al.* Deep brain stimulation for treatment-resistant depression. *Neuron* **45**, 651-660 (2005). https://doi.org:10.1016/j.neuron.2005.02.014

5 Disner, S. G., Beevers, C. G., Haigh, E. A. P. & Beck, A. T. Neural mechanisms of the cognitive model of depression. *Nat Rev Neurosci* **12**, 467-477 (2011).

6 Cash, R. F. H. *et al.* Using Brain Imaging to Improve Spatial Targeting of Transcranial Magnetic Stimulation for Depression. *Biol Psychiatry* (2020). https://doi.org:10.1016/j.biopsych.2020.05.033

7 Fitzgerald, P. B. Targeting repetitive transcranial magnetic stimulation in depression: do we really know what we are stimulating and how best to do it? *Brain Stimul* **14**, 730-736 (2021). https://doi.org:10.1016/j.brs.2021.04.018

8 Connolly, C. G. *et al.* Resting-State Functional Connectivity of Subgenual Anterior Cingulate Cortex in Depressed Adolescents. *Biological Psychiatry* **74**, 898-907 (2013). https://doi.org:http://dx.doi.org/10.1016/j.biopsych.2013.05.036

9 Greicius, M. D. *et al.* Resting-state functional connectivity in major depression: abnormally increased contributions from subgenual cingulate cortex and thalamus. *Biol Psychiatry* **62**, 429-437 (2007). https://doi.org:10.1016/j.biopsych.2006.09.020

10 Wu, H. *et al.* Changed Hub and Corresponding Functional Connectivity of Subgenual Anterior Cingulate Cortex in Major Depressive Disorder. *Front Neuroanat* **10**, 120 (2016). https://doi.org:10.3389/fnana.2016.00120

11 Davey, C. G., Harrison, B. J., Yucel, M. & Allen, N. B. Regionally specific alterations in

715 functional connectivity of the anterior cingulate cortex in major depressive disorder.
716 *Psychol Med* **42**, 2071-2081 (2012). https://doi.org:10.1017/s0033291712000323
717 12 Cheng, B. *et al.* Functional connectivity patterns of the subgenual anterior cingulate
718 cortex in first-episode refractory major depressive disorder. *Brain imaging and*
719 *behavior* **15**, 2397-2405 (2021). https://doi.org:10.1007/s11682-020-00436-x
720 13 Sheline, Y. I., Price, J. L., Yan, Z. & Mintun, M. A. Resting-state functional MRI in
721 depression unmasks increased connectivity between networks via the dorsal nexus.
722 *Proc Natl Acad Sci U S A* **107**, 11020-11025 (2010).
723 https://doi.org:10.1073/pnas.1000446107
724 14 Berman, M. G. *et al.* Depression, rumination and the default network. *Social*
725 *cognitive and affective neuroscience* **6**, 548-555 (2011).
726 https://doi.org:10.1093/scan/nsq080
727 15 Wu, X. *et al.* Dysfunction of the cingulo-opercular network in first-episode
728 medication-naive patients with major depressive disorder. *J Affect Disord* **200**,
729 275-283 (2016). https://doi.org:10.1016/j.jad.2016.04.046
730 16 Sudheimer, K. *et al.* Decreased hypothalamic functional connectivity with subgenual
731 cortex in psychotic major depression. *Neuropsychopharmacology* **40**, 849-860 (2015).
732 https://doi.org:10.1038/npp.2014.259
733 17 Davey, C. G., Yücel, M., Allen, N. B. & Harrison, B. J. Task-related deactivation and
734 functional connectivity of the subgenual cingulate cortex in major depressive
735 disorder. *Frontiers in psychiatry* **3**, 14 (2012).
736 https://doi.org:10.3389/fpsyt.2012.00014
737 18 Gaffrey, M. S. *et al.* Subgenual cingulate connectivity in children with a history of
738 preschool-depression. *Neuroreport* **21**, 1182-1188 (2010).
739 https://doi.org:10.1097/WNR.0b013e32834127eb
740 19 Ho, T. C. *et al.* Functional connectivity of negative emotional processing in adolescent
741 depression. *J Affect Disord* **155**, 65-74 (2014).
742 https://doi.org:10.1016/j.jad.2013.10.025
743 20 Button, K. S. *et al.* Power failure: why small sample size undermines the reliability of
744 neuroscience. *Nat Rev Neurosci* **14**, 365-376 (2013).
745 https://doi.org:10.1038/nrn3475
746 21 Algermissen, J. & Mehler, D. M. A. May the power be with you: are there highly
747 powered studies in neuroscience, and how can we get more of them? *J Neurophysiol*
748 **119**, 2114-2117 (2018). https://doi.org:10.1152/jn.00765.2017
749 22 Chen, X. *et al.* The DIRECT consortium and the REST-meta-MDD project: towards
750 neuroimaging biomarkers of major depressive disorder. *Psychoradiology* **2**, 32-42
751 (2022). https://doi.org:10.1093/psyrad/kkac005
752 23 Yan, C. G. *et al.* Reduced default mode network functional connectivity in patients
753 with recurrent major depressive disorder. *Proc Natl Acad Sci U S A* (2019).
754 https://doi.org:10.1073/pnas.1900390116
755 24 Schmaal, L. *et al.* ENIGMA MDD: seven years of global neuroimaging studies of major
756 depression through worldwide data sharing. *Transl Psychiatry* **10**, 172 (2020).
757 https://doi.org:10.1038/s41398-020-0842-6

25 Yang, H. *et al.* Disrupted intrinsic functional brain topology in patients with major depressive disorder. *Mol Psychiatry* (2021). https://doi.org:10.1038/s41380-021-01247-2

26 Long, Y. *et al.* Altered resting-state dynamic functional brain networks in major depressive disorder: Findings from the REST-meta-MDD consortium. *Neuroimage Clin* **26**, 102163 (2020). https://doi.org:10.1016/j.nicl.2020.102163

27 Ding, Y. D. *et al.* Disrupted hemispheric connectivity specialization in patients with major depressive disorder: Evidence from the REST-meta-MDD Project. *J Affect Disord* **284**, 217-228 (2021). https://doi.org:10.1016/j.jad.2021.02.030

28 Deng, K. *et al.* Impaired robust interhemispheric function integration of depressive brain from REST-meta-MDD database in China. *Bipolar disorders* (2021). https://doi.org:10.1111/bdi.13139

29 Liang, S. *et al.* Biotypes of major depressive disorder: Neuroimaging evidence from resting-state default mode network patterns. *Neuroimage Clin* **28**, 102514 (2020). https://doi.org:10.1016/j.nicl.2020.102514

30 Liu, P. H. *et al.* Brain structural alterations in MDD patients with gastrointestinal symptoms: Evidence from the REST-meta-MDD project. *Progress in neuro-psychopharmacology & biological psychiatry* **111**, 110386 (2021). https://doi.org:10.1016/j.pnpbp.2021.110386

31 Yan, C.-G., Wang, X.-D. & Lu, B. DPABISurf: data processing & analysis for brain imaging on surface. *Science Bulletin* (2021). https://doi.org:https://doi.org/10.1016/j.scib.2021.09.016

32 Ge, R., Downar, J., Blumberger, D. M., Daskalakis, Z. J. & Vila-Rodriguez, F. Functional connectivity of the anterior cingulate cortex predicts treatment outcome for rTMS in treatment-resistant depression at 3-month follow-up. *Brain Stimul* **13**, 206-214 (2020). https://doi.org:10.1016/j.brs.2019.10.012

33 Cash, R. F. H. *et al.* A multivariate neuroimaging biomarker of individual outcome to transcranial magnetic stimulation in depression. *Hum Brain Mapp* **40**, 4618-4629 (2019). https://doi.org:10.1002/hbm.24725

34 Philip, N. S. *et al.* Network Mechanisms of Clinical Response to Transcranial Magnetic Stimulation in Posttraumatic Stress Disorder and Major Depressive Disorder. *Biol Psychiatry* **83**, 263-272 (2018). https://doi.org:10.1016/j.biopsych.2017.07.021

35 Fox, M. D., Buckner, R. L., White, M. P., Greicius, M. D. & Pascual-Leone, A. Efficacy of transcranial magnetic stimulation targets for depression is related to intrinsic functional connectivity with the subgenual cingulate. *Biol Psychiatry* **72**, 595-603 (2012). https://doi.org:10.1016/j.biopsych.2012.04.028

36 Elbau, I. G. *et al.* Functional Connectivity Mapping for rTMS Target Selection in Depression. *Am J Psychiatry* **180**, 230-240 (2023). https://doi.org:10.1176/appi.ajp.20220306

37 Weigand, A. *et al.* Prospective Validation That Subgenual Connectivity Predicts Antidepressant Efficacy of Transcranial Magnetic Stimulation Sites. *Biol Psychiatry* **84**, 28-37 (2018). https://doi.org:10.1016/j.biopsych.2017.10.028

38 Cash, R. F. H., Cocchi, L., Lv, J., Fitzgerald, P. B. & Zalesky, A. Functional Magnetic

801 Resonance Imaging-Guided Personalization of Transcranial Magnetic Stimulation
802 Treatment for Depression. *JAMA psychiatry* **78**, 337-339 (2021).
803 https://doi.org:10.1001/jamapsychiatry.2020.3794
804 39 Siddiqi, S. H., Weigand, A., Pascual-Leone, A. & Fox, M. D. Identification of
805 Personalized Transcranial Magnetic Stimulation Targets Based on Subgenual
806 Cingulate Connectivity: An Independent Replication. *Biol Psychiatry* **90**, e55-e56
807 (2021). https://doi.org:10.1016/j.biopsych.2021.02.015
808 40 Fox, M. D., Liu, H. & Pascual-Leone, A. Identification of reproducible individualized
809 targets for treatment of depression with TMS based on intrinsic connectivity.
810 *Neuroimage* **66**, 151-160 (2013). https://doi.org:10.1016/j.neuroimage.2012.10.082
811 41 Gordon, E. M. & Nelson, S. M. Three types of individual variation in brain networks
812 revealed by single-subject functional connectivity analyses. *Current Opinion in*
813 *Behavioral Sciences* **40**, 79-86 (2021).
814 42 Doucet, G. E., Lee, W. H. & Frangou, S. Evaluation of the spatial variability in the
815 major resting-state networks across human brain functional atlases. *Hum Brain*
816 *Mapp* **40**, 4577-4587 (2019). https://doi.org:10.1002/hbm.24722
817 43 Cash, R. F. H. *et al.* Personalized connectivity-guided DLPFC-TMS for depression:
818 Advancing computational feasibility, precision and reproducibility. *Hum Brain Mapp*
819 (2021). https://doi.org:10.1002/hbm.25330
820 44 Cole, E. J. *et al.* Stanford Neuromodulation Therapy (SNT): A Double-Blind
821 Randomized Controlled Trial. *Am J Psychiatry*, appiajp202120101429 (2021).
822 https://doi.org:10.1176/appi.ajp.2021.20101429
823 45 Cole, E. J. *et al.* Stanford Accelerated Intelligent Neuromodulation Therapy for
824 Treatment-Resistant Depression. *Am J Psychiatry* **177**, 716-726 (2020).
825 https://doi.org:10.1176/appi.ajp.2019.19070720
826 46 Williams, N. R. *et al.* High-dose spaced theta-burst TMS as a rapid-acting
827 antidepressant in highly refractory depression. *Brain* **141**, e18 (2018).
828 https://doi.org:10.1093/brain/awx379
829 47 Cash, R. F. H. *et al.* Subgenual Functional Connectivity Predicts Antidepressant
830 Treatment Response to Transcranial Magnetic Stimulation: Independent Validation
831 and Evaluation of Personalization. *Biological psychiatry* **86**, e5-e7 (2019).
832 https://doi.org:10.1016/j.biopsych.2018.12.002
833 48 Cash, R. F. H. *et al.* Personalized connectivity-guided DLPFC-TMS for depression:
834 Advancing computational feasibility, precision and reproducibility. *Hum Brain Mapp*
835 **42**, 4155-4172 (2021). https://doi.org:10.1002/hbm.25330
836 49 Ojemann, J. G. *et al.* Anatomic localization and quantitative analysis of gradient
837 refocused echo-planar fMRI susceptibility artifacts. *Neuroimage* **6**, 156-167 (1997).
838 https://doi.org:10.1006/nimg.1997.0289
839 50 Beckmann, C. F., Mackay, C. E., Filippini, N. & Smith, S. M. Group comparison of
840 resting-state FMRI data using multi-subject ICA and dual regression. *NeuroImage* **47**
841 (2009). https://doi.org:10.1016/s1053-8119(09)71511-3
842 51 Zuo, X. N. *et al.* Reliable intrinsic connectivity networks: test-retest evaluation using
843 ICA and dual regression approach. *Neuroimage* **49**, 2163-2177 (2010).

https://doi.org:10.1016/j.neuroimage.2009.10.080

52 Garza-Villarreal, E. A. *et al.* Clinical and Functional Connectivity Outcomes of 5-Hz Repetitive Transcranial Magnetic Stimulation as an Add-on Treatment in Cocaine Use Disorder: A Double-Blind Randomized Controlled Trial. *Biological psychiatry. Cognitive neuroscience and neuroimaging* **6**, 745-757 (2021). https://doi.org:10.1016/j.bpsc.2021.01.003

53 Team, R. C. *R: A language and environment for statistical computing*. (R Foundation for Statistical Computing, 2013).

54 Champely, S. *et al.* pwr: Basic functions for power analysis. (2017).

55 Yan, C.-G., Wang, X.-D., Zuo, X.-N. & Zang, Y.-F. DPABI: Data Processing & Analysis for (Resting-State) Brain Imaging. *Neuroinformatics* **14**, 339-351 (2016). https://doi.org:10.1007/s12021-016-9299-4

56 Yan, C.-G. & Zang, Y.-F. DPARSF: A MATLAB Toolbox for "Pipeline" Data Analysis of Resting-State fMRI. *Frontiers in systems neuroscience* **4**, 13 (2010). https://doi.org:10.3389/fnsys.2010.00013

57 Liston, C. *et al.* Default mode network mechanisms of transcranial magnetic stimulation in depression. *Biol Psychiatry* **76**, 517-526 (2014). https://doi.org:10.1016/j.biopsych.2014.01.023

58 Johnson, W. E., Li, C. & Rabinovic, A. Adjusting batch effects in microarray expression data using empirical Bayes methods. *Biostatistics* **8**, 118-127 (2007). https://doi.org:10.1093/biostatistics/kxj037

59 Greicius, M. Resting-state functional connectivity in neuropsychiatric disorders. *Current opinion in neurology* **21**, 424-430 (2008). https://doi.org:10.1097/WCO.0b013e328306f2c5

60 Cullen, K. R. *et al.* A preliminary study of functional connectivity in comorbid adolescent depression. *Neuroscience Letters* **460**, 227-231 (2009). https://doi.org:http://dx.doi.org/10.1016/j.neulet.2009.05.022

61 Strikwerda-Brown, C. *et al.* Mapping the relationship between subgenual cingulate cortex functional connectivity and depressive symptoms across adolescence. *Social cognitive and affective neuroscience* **10**, 961-968 (2015). https://doi.org:10.1093/scan/nsu143

62 Ioannidis, J. P. A. Why Most Published Research Findings Are False. *PLOS Medicine* **2**, e124 (2005). https://doi.org:10.1371/journal.pmed.0020124

63 Chen, X., Lu, B. & Yan, C. G. Reproducibility of R-fMRI metrics on the impact of different strategies for multiple comparison correction and sample sizes. *Hum Brain Mapp* **39**, 300-318 (2018). https://doi.org:10.1002/hbm.23843

64 Price, J. L. & Drevets, W. C. Neurocircuitry of mood disorders. *Neuropsychopharmacology* **35**, 192-216 (2010). https://doi.org:10.1038/npp.2009.104

65 Price, J. L. & Drevets, W. C. Neural circuits underlying the pathophysiology of mood disorders. *Trends Cogn Sci* **16**, 61-71 (2012). https://doi.org:10.1016/j.tics.2011.12.011

66 Hamilton, J. P., Farmer, M., Fogelman, P. & Gotlib, I. H. Depressive Rumination, the

887 Default-Mode Network, and the Dark Matter of Clinical Neuroscience. *Biol Psychiatry*
888 **78**, 224-230 (2015). https://doi.org:10.1016/j.biopsych.2015.02.020
889 67 Parker, G., Chan, B. & Hadzi-Pavlovic, D. Lower rates of depression in westernised
890 Chinese in the US. *J Affect Disord* **104**, 175-178 (2007).
891 https://doi.org:10.1016/j.jad.2007.02.020
892 68 Parker, G., Gladstone, G. & Chee, K. T. Depression in the planet's largest ethnic group:
893 the Chinese. *Am J Psychiatry* **158**, 857-864 (2001).
894 https://doi.org:10.1176/appi.ajp.158.6.857
895 69 Qiu, P., Caine, E. D., Hou, F., Cerulli, C. & Wittink, M. N. Depression as seen through
896 the eyes of rural Chinese women: Implications for help-seeking and the future of
897 mental health care in China. *J Affect Disord* **227**, 38-47 (2018).
898 https://doi.org:10.1016/j.jad.2017.10.016
899 70 Kiyohara, C. & Yoshimasu, K. Association between major depressive disorder and a
900 functional polymorphism of the 5-hydroxytryptamine (serotonin) transporter gene: a
901 meta-analysis. *Psychiatr Genet* **20**, 49-58 (2010).
902 https://doi.org:10.1097/YPG.0b013e328335112b
903 71 Fitzgerald, P. B. *et al.* An analysis of functional neuroimaging studies of dorsolateral
904 prefrontal cortical activity in depression. *Psychiatry Res* **148**, 33-45 (2006).
905 https://doi.org:10.1016/j.pscychresns.2006.04.006
906 72 Rajkowska, G. & Goldman-Rakic, P. S. Cytoarchitectonic definition of prefrontal areas
907 in the normal human cortex: II. Variability in locations of areas 9 and 46 and
908 relationship to the Talairach Coordinate System. *Cerebral cortex (New York, N.Y. :*
909 *1991)* **5**, 323-337 (1995). https://doi.org:10.1093/cercor/5.4.323
910 73 Johnson, K. A. *et al.* Prefrontal rTMS for treating depression: location and intensity
911 results from the OPT-TMS multi-site clinical trial. *Brain Stimul* **6**, 108-117 (2013).
912 https://doi.org:10.1016/j.brs.2012.02.003
913 74 Perera, T. *et al.* The Clinical TMS Society Consensus Review and Treatment
914 Recommendations for TMS Therapy for Major Depressive Disorder. *Brain Stimul* **9**,
915 336-346 (2016). https://doi.org:10.1016/j.brs.2016.03.010
916 75 Fitzgerald, P. B. *et al.* A randomized trial of rTMS targeted with MRI based
917 neuro-navigation in treatment-resistant depression. *Neuropsychopharmacology* **34**,
918 1255-1262 (2009). https://doi.org:10.1038/npp.2008.233
919 76 Hebel, T. *et al.* A direct comparison of neuronavigated and non-neuronavigated
920 intermittent theta burst stimulation in the treatment of depression. *Brain Stimul* **14**,
921 335-343 (2021). https://doi.org:10.1016/j.brs.2021.01.013
922 77 Modak, A. & Fitzgerald, P. B. Personalising transcranial magnetic stimulation for
923 depression using neuroimaging: A systematic review. *The World Journal of Biological*
924 *Psychiatry* **22**, 647-669 (2021). https://doi.org:10.1080/15622975.2021.1907710
925 78 Dubois, J. & Adolphs, R. Building a Science of Individual Differences from fMRI.
926 *Trends in Cognitive Sciences* **20**, 425-443 (2016).
927 https://doi.org:http://dx.doi.org/10.1016/j.tics.2016.03.014
928 79 Zuo, X. N. & Xing, X. X. Test-retest reliabilities of resting-state FMRI measurements in
929 human brain functional connectomics: a systems neuroscience perspective. *Neurosci*

Biobehav Rev **45**, 100-118 (2014). https://doi.org:10.1016/j.neubiorev.2014.05.009

80 Zald, D. H. & Rauch, S. *The orbitofrontal cortex*. (Oxford University Press, USA, 2006).

81 Siddiqi, S. H. *et al.* Repetitive Transcranial Magnetic Stimulation with Resting-State Network Targeting for Treatment-Resistant Depression in Traumatic Brain Injury: A Randomized, Controlled, Double-Blinded Pilot Study. *J Neurotrauma* **36**, 1361-1374 (2019). https://doi.org:10.1089/neu.2018.5889

82 Schmaal, L. *et al.* Cortical abnormalities in adults and adolescents with major depression based on brain scans from 20 cohorts worldwide in the ENIGMA Major Depressive Disorder Working Group. *Mol Psychiatry* (2016). https://doi.org:10.1038/mp.2016.60

83 Schmaal, L. *et al.* Subcortical brain alterations in major depressive disorder: findings from the ENIGMA Major Depressive Disorder working group. *Mol Psychiatry* **21**, 806-812 (2016). https://doi.org:10.1038/mp.2015.69

84 Esteban, O. *et al.* fMRIPrep: a robust preprocessing pipeline for functional MRI. *Nat Methods* **16**, 111-116 (2019). https://doi.org:10.1038/s41592-018-0235-4

85 Lynch, C. J. *et al.* Automated optimization of TMS coil placement for personalized functional network engagement. *Neuron* **110**, 3263-3277.e3264 (2022). https://doi.org:10.1016/j.neuron.2022.08.012

86 Downar, J. & Daskalakis, Z. J. New targets for rTMS in depression: a review of convergent evidence. *Brain Stimul* **6**, 231-240 (2013). https://doi.org:10.1016/j.brs.2012.08.006

87 Siddiqi, S. H., Khosravani, S., Rolston, J. D. & Fox, M. D. The future of brain circuit-targeted therapeutics. *Neuropsychopharmacology* (2023). https://doi.org:10.1038/s41386-023-01670-9

88 Zuo, X.-N. & Xing, X.-X. Test-retest reliabilities of resting-state FMRI measurements in human brain functional connectomics: A systems neuroscience perspective. *Neuroscience & Biobehavioral Reviews* **45**, 100-118 (2014). https://doi.org:http://dx.doi.org/10.1016/j.neubiorev.2014.05.009

89 Wang, D. *et al.* Parcellating cortical functional networks in individuals. *Nat Neurosci* **18**, 1853-1860 (2015). https://doi.org:10.1038/nn.4164

90 Dunlop, K. *et al.* Dorsomedial prefrontal cortex repetitive transcranial magnetic stimulation for treatment-refractory major depressive disorder: A three-arm, blinded, randomized controlled trial. *Brain Stimul* **13**, 337-340 (2020). https://doi.org:10.1016/j.brs.2019.10.020

966 Table 1. Demographic data for all samples included in the DIRECT II project

Site	Age (HC)[1]	Age (MDD)[1]	% Male (HC)[2]	% Female (HC)[2]	% Male (MDD)[2]	% Female (MDD)[2]	Education (HC, years)[1]	Education (MDD, years)[1]	N (HC)	N (MDD)
1	39.33 (15.80)	38.67 (13.50)	87 (35.22%)	160 (64.78%)	98 (35.13%)	181 (64.87%)	13.05 (3.89)	12.03 (3.62)	247	279
2	20.90 (2.89)	19.02 (3.79)	24 (38.71%)	38 (61.29%)	37 (27.41%)	98 (72.59%)	13.73 (1.80)	11.97 (2.55)	62	135
3	26.50 (11.22)	34.40 (10.56)	5 (25.00%)	15 (75.00%)	5 (25.00%)	15 (75.00%)	15.40 (1.47)	14.90 (2.97)	20	20
4	29.89 (9.88)	30.87 (10.39)	9 (33.33%)	18 (66.67%)	13 (41.94%)	18 (58.06%)	13.04 (3.80)	12.65 (4.22)	27	31
5	36.79 (9.07)	33.59 (9.85)	32 (56.14%)	25 (43.86%)	60 (46.88%)	68 (53.13%)	14.37 (2.64)	13.07 (3.43)	57	128
6	23.75 (5.15)	30.90 (9.29)	45 (44.55%)	56 (55.45%)	31 (52.54%)	28 (47.46%)	13.88 (2.31)	12.03 (3.06)	101	59
7	19.80 (3.85)	20.00 (6.51)	8 (26.67%)	22 (73.33%)	5 (23.81%)	16 (76.19%)	11.90 (2.55)	10.81 (2.86)	30	21
8	31.93 (9.66)	32.84 (8.95)	18 (42.86%)	24 (57.14%)	15 (34.88%)	28 (65.12%)	15.40 (1.86)	15.79 (1.82)	42	43
9	36.12 (13.85)	45.11 (14.32)	10 (40.00%)	15 (60.00%)	19 (40.43%)	28 (59.57%)	13.56 (4.01)	10.83 (4.52)	25	47
10	36.49 (12.64)	34.00 (11.81)	30 (44.78%)	37 (55.22%)	36 (45.00%)	44 (55.00%)	14.58 (2.30)	13.25 (3.08)	67	80
11	36.62 (12.11)	38.29 (12.75)	30 (44.12%)	38 (55.88%)	55 (48.67%)	58 (51.33%)	12.96 (3.57)	10.96 (3.48)	68	113
12	29.59 (5.00)	30.47 (7.20)	15 (46.88%)	17 (53.13%)	21 (33.87%)	41 (66.13%)	14.59 (2.82)	13.73 (3.39)	32	62
13	35.45 (13.76)	38.00 (14.56)	9 (31.03%)	20 (68.97%)	13 (40.63%)	19 (59.38%)	11.28 (4.31)	12.03 (3.87)	29	32
14	38.10 (11.96)	43.50 (11.28)	65 (45.14%)	79 (54.86%)	47 (34.56%)	89 (65.44%)	13.24 (4.20)	9.07 (3.60)	144	136
15	21.51 (4.58)	22.06 (4.70)	23 (65.71%)	12 (34.29%)	7 (20.59%)	27 (79.41%)	12.57 (1.42)	11.85 (2.39)	35	34

16	25.73 (7.38)	26.07 (7.66)	44 (54.32%)	37 (45.68%)	37 (44.58%)	46 (55.42%)	15.53 (2.81)	13.81 (2.60)	81	83
17	34.73 (9.66)	35.21 (9.43)	19 (38.78%)	30 (61.22%)	15 (35.71%)	27 (64.29%)	14.31 (4.21)	12.50 (4.09)	49	42
18	32.19 (11.83)	35.25 (13.15)	13 (40.63%)	19 (59.38%)	12 (50.00%)	12 (50.00%)	12.53 (3.03)	13.42 (4.47)	32	24
19	30.94 (7.32)	27.03 (11.04)	16 (50.00%)	16 (50.00%)	5 (15.63%)	27 (84.38%)	13.94 (2.84)	12.69 (3.18)	32	32
20	31.40 (10.99)	27.80 (8.99)	5 (25.00%)	15 (75.00%)	4 (20.00%)	16 (80.00%)	16.10 (3.21)	13.60 (4.36)	20	20
21	32.80 (11.06)	32.52 (11.44)	31 (55.36%)	25 (44.64%)	17 (28.33%)	43 (71.67%)	15.88 (4.59)	12.20 (4.12)	56	60
22	34.67 (13.54)	35.74 (10.02)	8 (33.33%)	16 (66.67%)	10 (28.57%)	25 (71.43%)	14.21 (2.86)	13.20 (3.75)	24	35
23	13.57 (2.18)	13.91 (1.48)	14 (50.00%)	14 (50.00%)	8 (13.79%)	50 (86.21%)	7.57 (2.18)	7.91 (1.48)	28	58

1 Mean (SD)

2 N (%)